PCCP

PAPER

View Article Online
View Journal | View Issue

Cite this: *Phys. Chem. Chem. Phys.*, 2015, **17**, 31117

Polyphenylsilole multilayers – an insight from X-ray electron spectroscopy and density functional theory†

Katharina Diller,‡*[a] Yong Ma,§[b] Yi Luo,[b] Francesco Allegretti,[a] Jianzhao Liu,[c] Ben Zhong Tang,[c] Nian Lin,*[d] Johannes V. Barth[a] and Florian Klappenberger*[a]

Received 21st May 2015,
Accepted 19th October 2015

DOI: 10.1039/c5cp02935j

www.rsc.org/pccp

We present a combined investigation by means of X-ray photoelectron spectroscopy (XPS) and near-edge X-ray absorption fine-structure (NEXAFS) spectroscopy of condensed multilayers of two polyphenylsiloles, namely hexaphenylsilole (HPS) and tetraphenylsilole (TPS). Both compounds exhibit very similar spectroscopic signatures, whose interpretation is aided by density functional theory (DFT) calculations. High-resolution XPS spectra of the Si 2p and C 1s core levels of these multilayers indicate a positively charged silicon ion flanked by two negatively charged adjacent carbon atoms in the silole core of both molecules. This result is corroborated quantitatively by DFT calculations on isolated HPS (TPS) molecules, which show a natural bond orbital partial charge of +1.67 *e* (+1.58 *e*) on the silicon and −0.34 *e* (−0.58 *e*) on the two neighbouring carbon atoms in the silole ring. These charges are conserved in direct contact with a Cu(111) substrate for films of submonolayer coverage, as evidenced by the Si 2p XPS data. The C K-edge NEXAFS spectra of HPS and TPS multilayers exhibit distinct and differing features. Their main characteristics reappear in the simulated spectra and are assigned to the different inequivalent carbon species in the molecule. The angle-dependent measurements hardly reveal any dichroism, *i.e.*, the molecular π-systems are not uniformly oriented parallel or perpendicular with respect to the surface. Changes in the growth conditions of TPS, *i.e.*, a reduction of the substrate temperature from 240 K to 80 K during deposition, lead to a broadening of both XPS and NEXAFS signatures, as well as an upward shift of the Si 2p and C 1s binding energies, indicative of a less ordered growth mode at low temperature.

1 Introduction

Polyphenylsiloles are a group of organic compounds containing a silacyclopentadiene (silole) core which is attached to a varying number of phenyl rings. Compared to cyclopentadiene and heterocyclic compounds such as pyrrole, furan, or thiophene the silole core features a characteristic low-lying LUMO (lowest unoccupied molecular orbital) level,[1] *i.e.*, it has high electron-accepting properties. Siloles are known for their photoluminescence properties, which make them ideal candidates for use in organic light emitting diodes (OLEDs) or photovoltaics.[2] Of special importance is hereby the fact that, at variance with other compounds, they do not suffer from aggregation quenching, *i.e.*, the quenching of light emission when progressing from the solvent to solid state.

In contrast, enhanced light emission was found for aggregated siloles,[3,4] which can not only be exploited in opto-electronic devices, but also in chemical or biomacromolecular sensors.[2] One of the first synthesized siloles is 1,1,2,3,4,5-hexaphenylsilole (HPS)[5] (Fig. 1a), where each atom in the silole core is connected to at least one phenyl ring. It has attracted interest as it could be shown that HPS-based OLED-devices are very efficient.[6,7] Inherently, those studies focused on determining the fluorescence quantum yields of HPS films,[8] the charge carrier transport properties[9] and the position of the HOMO and LUMO levels. Until recently, there were surprisingly no reports on core-level spectroscopy of HPS films. In ref. 10 we used X-ray photoelectron spectroscopy (XPS) to follow the temperature-induced bond cleavage of HPS adsorbed onto Cu(111), but never performed a

[a] *Physik-Department, E20, Technische Universität München, 85748 Garching, Germany. E-mail: katharina.diller@tum.de, florian.klappenberger@tum.de*
[b] *Division of Theoretical Chemistry and Biology, School of Biotechnology, Royal Institute of Technology, S-106 91 Stockholm, Sweden*
[c] *Department of Chemistry, The Hong Kong University of Science and Technology, Clear Water Bay, Hong Kong, China*
[d] *Department of Physics, The Hong Kong University of Science and Technology, Clear Water Bay, Hong Kong, China. E-mail: phnlin@ust.hk*

† Electronic supplementary information (ESI) available. See DOI: 10.1039/c5cp02935j

‡ Current address: Institute of Condensed Matter Physics (ICMP), École polytechnique fédérale de Lausanne (EPFL), CH-1015 Lausanne, Switzerland.
§ Current address: School of Physics and Electronics, Shandong Normal University, Jinan, Shandong 250014, People's Republic of China.

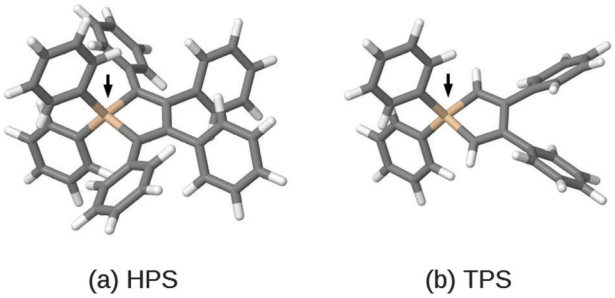

Fig. 1 Optimized geometries of (a) hexaphenylsilole (HPS) and (b) tetraphenylsilole (TPS). The silicon atom is marked by an arrow.

full spectroscopic analysis of the compound itself. Here, we characterise *in vacuo* deposited HPS multilayer films using XPS and near-edge X-ray absorption fine-structure (NEXAFS) spectroscopy measurements, complemented by density functional theory (DFT) simulations.

Using XPS and DFT we show that the silole core exhibits a positively charged silicon ion surrounded by negatively charged carbon species. A second polyphenylsilole, namely 1,1,3,4-tetraphenylsilole (TPS, Fig. 1b) possesses very similar properties indicating that this intramolecular charge distribution is a generic characteristic of silacyclopentadiene in polyphenylsiloles, regardless of the number of attached phenyl rings. In the second part of the study the NEXAFS signatures of HPS and TPS are assigned by using DFT. Polarization-dependent NEXAFS measurements do not show any dichroism for both multilayered samples, indicating that the molecular π-systems are not uniformly oriented parallel or perpendicular with respect to the surface.

2 Experimental and computational details

2.1 Experimental

The experimental data were obtained at the synchrotron BESSY-II in Berlin at the undulator beamlines U49/2 PGM-1 (HPS) and U49/2 PGM-2 (TPS), which provide beams with high flux and good energy resolution (typical resolution of the setup is 0.10 to 0.15 eV). All experiments were performed in a custom-designed ultrahigh vacuum chamber with base pressure in the high 10^{-11} mbar regime, equipped with a hemispherical electron energy analyser (SPECS Phoibos 100 CCD), a partial yield detector, and all ancillary facilities for sample preparation and characterisation.

The polyphenylsilole multilayers were grown on a Cu(111) single crystal whose surface was prepared by repeated cycles of Ar^+ and Ne^+ sputtering at 1 keV and subsequent annealing at 720 K. The HPS and TPS molecules were deposited by organic molecular beam epitaxy from a boron nitride crucible held at 380 K onto the substrate which was kept at 80–240 K. Prior to the experiments the molecules were degassed *in vacuo* by heating them up for several hours.

All XPS measurements were performed in a grazing incidence (7°) – normal emission geometry; a photon energy of 199 eV was used for Si 2p and 385 eV for the C 1s measurements. Binding energies were either referenced against the Cu $3p_{3/2}$ line (at 75.1 eV (ref. 11)) or the Fermi-edge of the substrate. After subtracting a linear background from the raw data, the spectra were fitted using Voigt curves.

NEXAFS data were taken in the partial electron yield (PEY) mode with a retarding voltage of −30 V for the Si L-edge and −200 V for the C K-edge. The incidence angle θ between the surface normal and the electric field of the linearly polarised light was varied from 7° to 90° by rotating the sample with respect to the incoming beam. After calibrating the photon energy scale, the signal of a bare Cu(111) crystal was subtracted from the sample spectrum, followed by a correction for the photon flux and a normalization of the edge jump to one (ref. 12).

2.2 Computational

The geometric structures of HPS and TPS were optimised at the DFT level using the B3LYP[13] functional and the 6-31g basis set by using the GAUSSIAN09 package.[14] The optimised geometries of these two molecules are shown in Fig. 1. Based on the optimised structures, C K-edge and Si L-edge XPS and NEXAFS spectra were calculated at the DFT level by using the StoBe program.[15] The ionisation potentials (IPs) of the non-equivalent atoms were calculated as the energy difference between the core-ionised and ground states (GS) from the ΔKohn–Sham (ΔKS) scheme.[16,17] The core-ionised states were approximated by the full core hole states (FCH). Then the XPS spectrum was obtained by weighted broadening of all the IPs with a Lorentzian function, whereby a full-width-at-half-maximum (FWHM) of 0.3 eV was used for XPS. The NEXAFS spectra were also calculated within the FCH approximation. The absorption oscillator strength for transition i → f is given by

$$I_{\mathrm{if}} = \frac{2m\varepsilon_{\mathrm{if}}}{3\hbar^2} \sum_{q=x,y,z} |\langle \psi_{\mathrm{f}}|q|\psi_{\mathrm{i}}\rangle|^2 \qquad (1)$$

where $\psi_{\mathrm{i,f}}$ denotes the two molecular orbitals involved in the transition, $\varepsilon_{\mathrm{if}}$ represents the corresponding orbital energy difference, and the summation over x, y, and z components accounts for the random orientation of molecules, *i.e.*, the magic angle of 55° in the measurement. Raw spectra were calibrated by the accurate energy value for the excitation from the 1s to LUMO transition. The calibrated discrete line was convoluted by Lorentzian functions with a FWHM of 0.6 eV below the IP. The Stieltjes imaging (SI)[18–20] method was applied to obtain the photoionisation cross-section in the continuum region. For the Si L edge, in particular, the spin–orbit split $2p_{1/2}$ and $2p_{3/2}$ components were approximately simulated by the calculated spectra of $2p_{x,y,z}$ with energy splitting of 0.6 eV and an intensity ratio of 1 : 2 (*cf.* ESI†). For the simulation of the spectra the exchange and correlation were described by the gradient corrected BE88[21] and PD86[22] functionals. In the computation, we employed a double basis set technique,[23] in which the triple-ζ quality individual gauge for localized orbital (IGLO-III) basis set[24] was used for the excited atom, and the triple-ζ plus valence polarisation (TZVP) basis set was used for the rest of the atoms.

To enable a direct comparison with the experiment, the energy scale of the simulated XPS and NEXAFS spectra was rigidly shifted (by 0.3 eV for C, 1.5 eV for Si of HPS, and 0.5 eV for Si of TPS) to match the position of the measured curves in Fig. 2, 4, 5, and Fig. S1 (ESI†).

Partial charges displayed in Fig. S2a and b (ESI†) were evaluated using the Mulliken[25] partitioning scheme. As the Mulliken analysis is known to be sensitive to the choice of the basis set,[26] for both compounds we additionally performed Natural Bond Orbital (NBO)[27] calculations as implemented in GAUSSIAN09.[14] All values are displayed and listed in the ESI.†

3 Results and discussion

3.1 XPS

X-ray photoelectron spectroscopy was used to characterise the polyphenylsilole multilayers with elemental and chemical sensitivity. In particular, XPS is perfectly suited to study the number and type of chemical species present in the sample, thanks to the known relationship between the measured binding energies and the oxidation state of silicon atoms[28,29] in different compounds. Thus, the growth of HPS (Fig. 2a) at 240 K on Cu(111) was monitored by XPS (Fig. 2c–h) in the Si 2p (left panel) and C 1s (right panel) regions. The Si 2p region of a HPS multilayer (Fig. 2c) shows a well-resolved Si 2p spin–orbit doublet (blue curves) with individual components centred at binding energies of 100.7 eV ($2p_{3/2}$) and 101.3 eV ($2p_{1/2}$) respectively.

These energies lie well above the values for neutral bulk silicon ($E_B(2p_{3/2})$ = 99.4 eV in ref. 11 and 99.6 eV in ref. 30), but agree well with that of, *e.g.*, the Si^+ ion in SiC (100.6 eV,[31] Si $2p_{3/2}$), thus pointing towards a positively charged silicon atom in the silole core. Our finding for HPS is therefore well in line with other organosilicon compounds where Mulliken charge analysis calculations predict a positive partial charge on the silicon.[32,33] For coverages in the sub-monolayer regime the Si 2p doublet is shifted by 0.3 eV to lower binding energies (Fig. 2g, green curves), which we attribute to a final-state effect arising from the polarisation screening of the core hole by electrons from the Cu(111) substrate.[34] Thus, the Si^+ state of the molecules is retained even for submonolayer coverages of HPS, likely because the adsorption geometry of the pristine molecule prevents a direct contact of the silicon ion with the Cu(111) substrate.[10] Correspondingly, the spectrum of a sample with a coverage of approximately 1.5 ML can be fitted with two doublets, reflecting the first and second layer contributions (Fig. 2e).

To get more quantitative information on the Si^+ state we additionally conducted DFT calculations on an isolated HPS molecule. The NBO (Mulliken) partial charge analysis of the silole core (Fig. 3a) does indeed find a positive charge of +1.67 *e* (+1.06 *e*) located at the silicon atom, which is in excellent agreement with what could be predicted from the experimental binding energies (according to ref. 35 and 36).

As to the C 1s region, the spectrum of the HPS multilayer (Fig. 2d) is dominated by a broad peak at 284.9 eV (grey striped component) which exhibits a small shoulder at lower binding

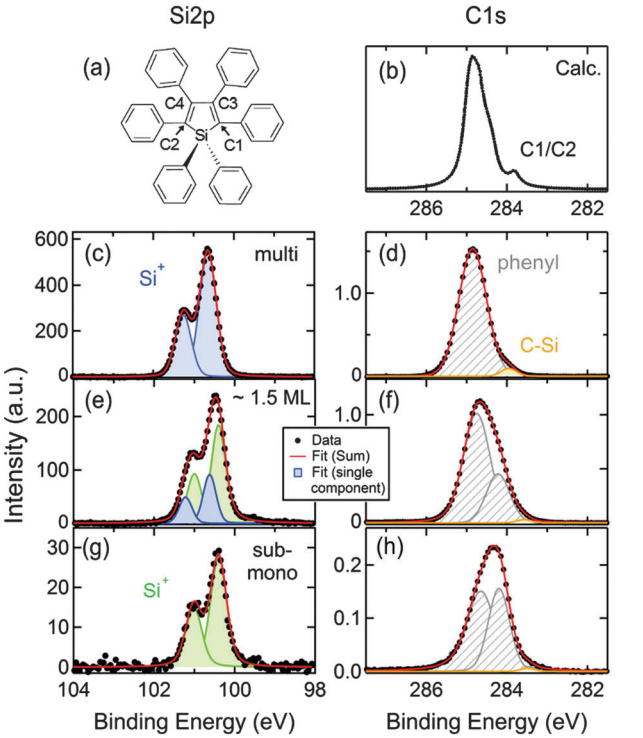

Fig. 2 Si 2p (left panel) and C 1s (right panel) XPS spectra of HPS. (a) Structural formula of HPS. The binding energy position of the Si 2p doublet for both HPS multilayer (c) and submonolayer (g) films is typical for the presence of Si^+ ions (see also calculated partial charges in Fig. 3a). The agreement between calculated (b) and experimental (d) C 1s spectra of the multilayer corroborates the assignment of the low energy contribution (orange) to C–Si bonds. The position of the low-energy feature points to partially negatively charged C1/C2 carbon atoms. The interaction with the surface leads to a change in the spectral shape (indicated by a fit with an additional phenyl component) for the lower coverages shown in (f) and (h).

energies (284.0 eV, orange component). The binding energy of the main peak is typical for carbon in conjugated environments (*e.g.*, 284.7 eV for phenylacetylene,[37] 285.1 eV for benzene,[38] 285.1 eV for polyphenyl-dicarbonitrile,[34] and 285.0 eV for phenyl rings attached to porphyrin macrocycles[39]) and is therefore assigned to signals from the carbon atoms in the phenyl rings. The shoulder clearly pertains to a different species. The comparison to the binding energy of carbon in SiC (283.1 eV[31]) suggests, consistent with the Si 2p data, slightly negatively charged carbon atoms are present in the silole core. The intensity ratio between the main peak and the shoulder in Fig. 2d lies between 17 : 1 and 29 : 1 (depending on the fit), indicating that two of the 40 carbon atoms carry a negative partial charge. The partial charge analysis confirms that indeed the two carbon atoms bonded to the silicon in the silole core (labelled as C1 and C2 in Fig. 2a) are slightly negatively charged (−0.40 *e* according to DFT). The good agreement between the multilayer data in Fig. 2d and the simulated C 1s XP spectrum of an isolated HPS molecule (2b) corroborates our peak assignment. Similarly to the Si 2p region the submonolayer spectrum (Fig. 2h) is shifted downwards with respect to that of the multilayer. Additionally, the shape of the main peak changes slightly and broadens

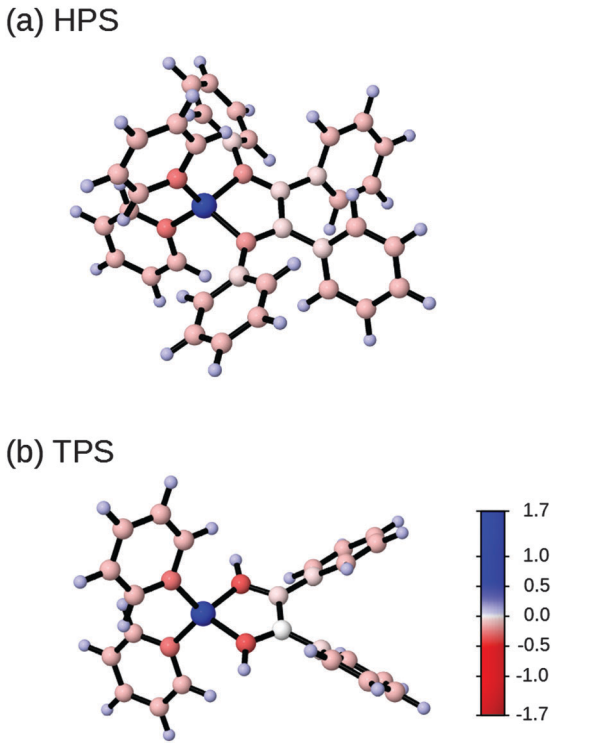

Fig. 3 Simulated NBO partial charges located at the individual atoms of the optimised geometries of (a) HPS and (b) TPS. Blue indicates positive and red negative charges. The most distinct feature, the clearly positive Si ion in the silole core which is flanked by negatively charged C atoms, of both molecules is in agreement with the binding energy positions of the Si 2p doublet and the C 1s low-energy shoulder (*cf.* Fig. 2 and 4).

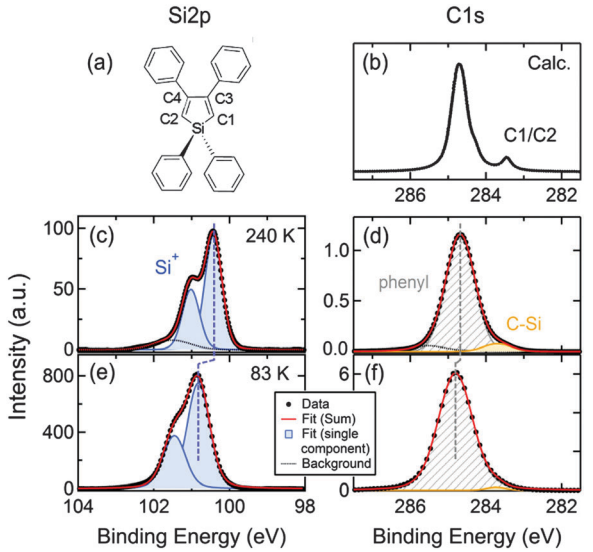

Fig. 4 Si 2p (left panel) and C 1s (right panel) XPS spectra of TPS multilayers (≥3 layers) grown at different substrate temperatures. (a) Structural formula of TPS. (b) Simulated C 1s spectrum. For temperatures close to room temperature (240 K) the shapes of both Si 2p (c) and C 1s (d) spectra are similar to those of HPS. Deposition at lower temperatures (e and f) leads to a general broadening of the spectroscopic features, indicating the presence of more than one distinct silicon species.

(illustrated by fitting with one additional component), which might be the consequence of different adsorption geometries (as described in ref. 40).

In the same way the smaller TPS molecule (Fig. 4a) was characterised: the Si 2p region of a TPS multilayer grown like HPS on the Cu(111) substrate kept at 240 K (Fig. 4c) shows a clearly separated spin–orbit doublet with individual components at 100.4 eV and 101.0 eV, respectively. The corresponding C 1s region (Fig. 4d) is very similar to that of HPS, but with a more pronounced shoulder (orange component). Following the same arguments presented for HPS, we conclude that the silicon atom is in a Si^+ state, while the two adjacent carbon atoms (C1/C2 in Fig. 4a) carry a negative charge. Indeed, the DFT NBO (Mulliken) analysis (Fig. 3b) reveals partial charges of +1.58 *e* (+0.96 *e*) (Si) and −0.58 *e* (−0.48 *e*) (C1/C2). The only relevant difference between the spectra of HPS and TPS, namely the decreased main peak to shoulder ratio (15 : 1) for the C 1s TPS spectra, is related to the smaller number of phenyl carbon atoms present in TPS. Even when changing the growth conditions (evaporation on a sputtered, non-annealed Cu(111) surface kept at 80 K), no new distinct features appear in the XPS spectra (Fig. 4e and f). We, however, observe a general broadening of all spectral features, as well as a slight upward shift of the C 1s curves, indicating less ordered layers with, presumably, molecules embedded in slightly different environments. The disentanglement of the spectra is non-trivial. While it would be possible to fit the Si 2p data with two sets of doublets (not shown), the C 1s spectrum would require the inclusion of a large amount of inequivalent chemical species and further reliable analysis is hampered.

3.2 NEXAFS

To gain more insight into the electronic structure and molecular orientation of HPS and TPS we conducted additional NEXAFS experiments and calculations at the C K-edge (Fig. 5) and the Si L-edge (Fig. 6 and ESI†). Measurements were conducted at two different orientations of the light electric field relative to the surface normal (7° and 90°). By making use of the fact that the intensity of the absorption spectra depends on the angle between the polarisation vector of the linearly polarised light and the final state orbital[41] it is possible to draw conclusions on the orientation of the molecules with respect to the surface. The number and position of peaks in the measured carbon spectra are nearly identical for HPS (Fig. 5b) and TPS (Fig. 5c): The dominating resonance at 285.1 eV (II) is preceded by a weaker feature (I) at 283.7 eV and followed by a double structure at higher photon energies (III, IV). II is typical for benzene resonance,[42] which is to be expected due to the presence of phenyl rings in our compounds. Peak I, however, is absent in the spectrum of benzene, and is therefore assigned to an excitation from the silole ring.

The peak assignment is confirmed by our DFT simulations resulting in the spectra of Fig. 5a and d. The good agreement between the experimental and theoretical curves directly allows an assignment of the observed features. The simulated C K-edge spectrum of HPS (Fig. 7a, black continuous line) reveals that even the asymmetric shape of peak II is reproduced

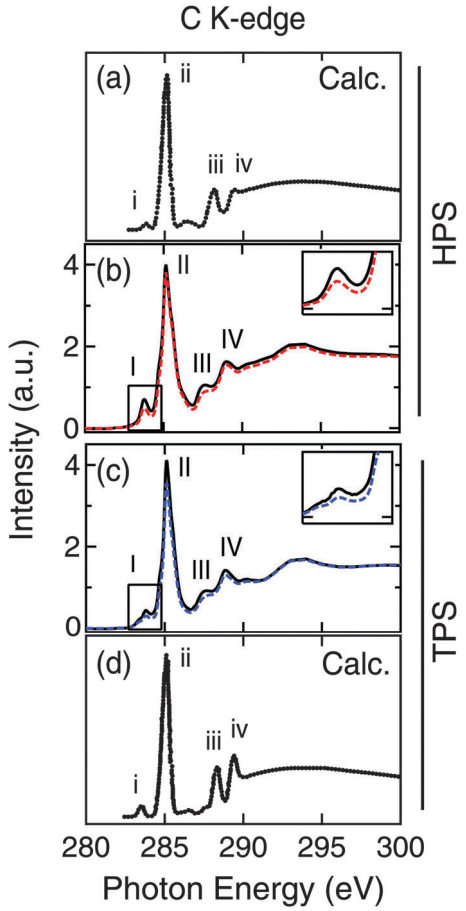

Fig. 5 Experimental and simulated NEXAFS C K-edge spectra of HPS (a and b) and TPS (c and d) multilayers. Both molecules exhibit similar spectroscopic signatures, *i.e.*, the number and position of resonances are nearly identical. For disentanglement of spectral signatures, see also Fig. 7.

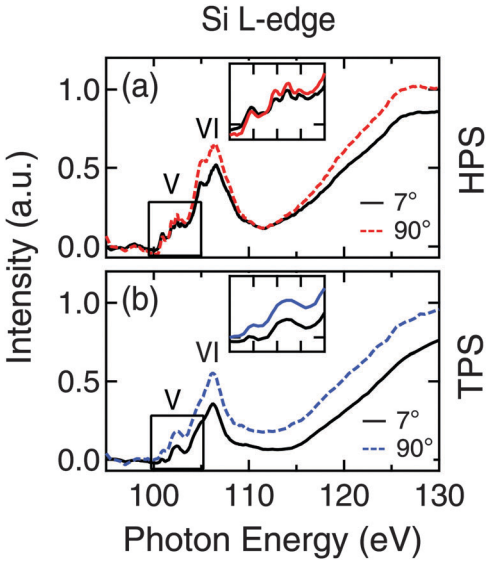

Fig. 6 Experimental Si L-edge spectra of HPS (a) and TPS (b) multilayers. Both molecules exhibit similar spectroscopic signatures, *i.e.*, the number and position of resonances are nearly identical. Some minor differences (see zoom-in shown in insets) might be related to different substrate temperatures during growth (240 K for HPS and 80 K for TPS), in agreement with the XPS data. Simulated spectra can be found in the ESI.†

by the simulation: the main peak is accompanied by both a low-energy shoulder and a higher-energy feature. The latter, however, appears as a shoulder in the experiment, but as a single feature in the simulation. The first peak (I) arises solely from the transition of the 1s states of C1 atoms (green dashed curve in Fig. 7a) of the silole core to the LUMO, which is mainly located at the silole ring, but also has contributions at the phenyl legs (Fig. 7c, inset). The main feature of the C1 spectrum (Fig. 7c) resembles that of benzene,[43] but is shifted to lower energies, mostly due to the lower lying 1s orbital of C1 which is reflected in the corresponding XPS peak position. Even though the silole atoms contribute, all other features are dominated by the phenyl contributions due to their relatively large number. It should be noted that the structure of the individual spectra of different carbon atoms mainly depends on the position of this atom in the respective subunit (indicated by arrows, circles and squares in Fig. 7), while the energy offset of the spectrum depends on the proximity to the silicon atom. As a general remark, the vanishing dichroism for both molecules rules out a layer-by-layer growth with exclusively flat (conformation A in ref. 40) or perpendicular silole cores and phenyl legs. However, the slightly different dichroism for peaks I and II might point towards an ensemble of ordered, albeit tilted molecules (*e.g.*, conformation B in ref. 40) rather than a purely random distribution, but the effect is so small that the issue cannot be conclusively addressed. Generally, the simulated curves in Fig. 5a and d agree very well with the corresponding experimental data, confirming that the recorded spectra truly reflect the polyphenylsiloles' spectral signatures in the multilayer and are barely influenced by molecule–molecule or even molecule–substrate interactions.

The Si L-edge spectra of HPS (Fig. 6a) and TPS (Fig. 6b) exhibit two main features V and VI. Moreover, for both molecules a substructure is present, which is reproduced by the calculation either as asymmetry in the main peaks V and VI (Fig. S1b, ESI†) or as a distinct splitting of feature V (Fig. S1d, ESI†). Even assuming a single silicon species in a well-defined chemical environment (as shown by XPS) the interpretation is not entirely straightforward as we have to account for spin–orbit splitting at the L-edge which is not present at the K-edge. The DFT code we employed does not account for spin–orbit splitting, thus our simulation of the Si L-edge is an approximation (see also ESI†) which makes use of the typical value for spin–orbit splitting derived from experiments of organosilicon compounds (0.63 eV for methylsilane[44] and 0.6 eV for silicon oxide[45]).

The more intense feature located between 104 and 109 eV (VI) is present in the NEXAFS L-edge spectra of various organosilicon compounds and was assigned to σ_{Si-C}^* and σ_{Si-O}^* transitions by Urquhart and co-workers.[46] For the compounds discussed in ref. 46 and 47 structure V (100.5–104 eV) is not present at all for the methyl-silicon compounds, while it is observed for compounds containing Si–phenyl bonds. Consistently, the latter were assigned to π_{Si-Ph}^* transitions.[46] The simulated Si L-edge NEXAFS data for HPS show that peak V

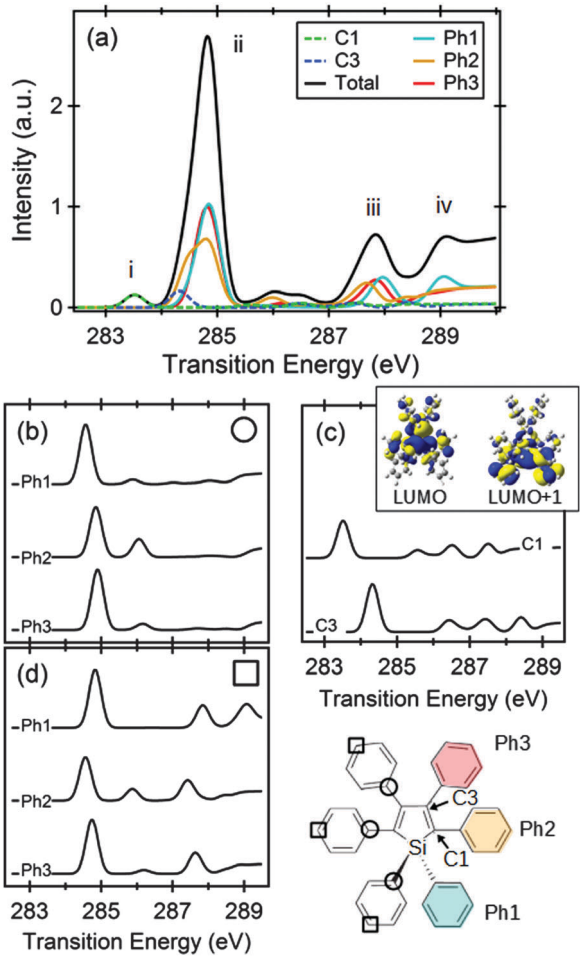

Fig. 7 Simulated C K-edge NEXAFS data for HPS. (a) Zoom-in of the total simulated curve (black) of Fig. 5a, together with the contributions from the silole core (C1 and C3, dashed lines) and the three phenyl rings (continuous lines). (b–d) A comparison of the single spectra of different individual carbon atoms in the HPS molecule (their positions are marked with arrows, circles and squares in the schematics on the right side). The inset in (c) displays the ground state LUMOs as simulated using DFT.

is mainly composed of 2p to LUMO+1 and 2p to LUMO+2 transitions. The low-energy shoulder of peak V originates from the transition from 2p to LUMO. The strong resonance labelled VI is mainly attributed to 2p to LUMO+13 transition.

For TPS the DFT results show that the split peak V can be assigned to the transitions of 2p to LUMO and 2p to LUMO+2. The resonance VI mainly originates from the 2p to LUMO+11 transition. It has to be noted that the experimental spectra of TPS show less sub-structures, even though the general shape is close to that observed for HPS. This can be easily explained by the fact that the TPS multilayer was grown at lower temperatures (80–240 K) on a non-annealed substrate, therefore leading to less ordered films with slightly inequivalent species due to the modified chemical environment (as shown by XPS). This seems plausible as it is known that even inert substrates such as Au(111) can influence the first layer of molecules in such a way that a highly-ordered multilayer growth is hindered.[48] The angular dependence of the spectra is similar for both molecules and seems to be slightly different from that of the carbon region. However, we refrain from discussing in more detail the angular dependence in the silicon region, as the recorded PEY signal is very small at the Si L-edge compared to the background, and the data processing proved to be non-trivial.

4 Conclusions

We employed two different experimental X-ray electron spectroscopy methods, namely XPS and NEXAFS, in conjunction with DFT calculations to characterise the polyphenylsilole molecules HPS and TPS, which consist of a silole ring attached to, respectively, six and four phenyl groups. The simulation of XP and NEXAFS spectra showed for both molecules a very good agreement with the corresponding measurements of HPS and TPS multilayers, underlining that in the thick layers the molecule–molecule interactions are weak. This allows us to gain information on the electronic state of pure compounds. For both molecules the position of the Si 2p XPS spin–orbit doublet is typical for silicon in a formal Si^{+} state. The appearance of a low-energy shoulder in the C 1s measurements points to the existence of negatively charged carbon atoms. These conclusions are confirmed by the DFT results using both Mulliken and NBO charge partitioning, which clearly show that in both compounds the silicon ion in the silole core carries a positive partial charge, whereas the adjacent carbon atoms are negatively charged. NEXAFS C K-edge measurements and simulations show a benzene-like spectrum with additional silole contributions at lower photon energies. The Si L-edge spectrum is characteristic of the molecules and can be separated into two structures containing π_{Si-Ph}^{*} and σ_{Si-C}^{*} contributions. Similar to the XPS fingerprint, the NEXAFS signatures for the two compounds are also very similar. Given the localized nature of the probed core levels, the lack of dependence of the photoelectron spectra on the number of attached phenyl rings is not surprising. For NEXAFS, in principle this does not need to be the case, as a modification of the compound may lead to additional final states, which would then appear as additional resonances in the spectrum. Our data, however, show that this is not the case for HPS and TPS, and that increasing the number of attached phenyl groups does not change the principal electronic structure. The weak angular dependence of the NEXAFS spectra for both molecules and regions rules out a layer-by-layer growth with exclusively flat or upright silole and phenyl groups. Changes in the growth conditions of TPS, *i.e.*, the change of the substrate temperature from 240 K to 80 K during deposition, lead to a broadening of both XPS and NEXAFS signatures, indicative of a less ordered growth mode.

Acknowledgements

This work was supported by the European Research Council (ERC Advanced Grant MolArt no. 247299), the Munich Centre for Advanced Photonics (MAP) funded by the German Research Foundation (DFG) *via* the German Excellence Initiative, the Hong

Kong RGC (grant HKUST2/CRF/10-B), and the DAAD (grant 423/hk-PPP-cab D/09/00810). The authors acknowledge the Helmholtz-Zentrum Berlin (Electron storage ring BESSY II) for provision of synchrotron radiation at beamlines U49/2 PGM-1 and U49/2 PGM-1. Covering the travelling cost for BESSY measurements by the Helmholtz-Zentrum Berlin is gratefully acknowledged. K.D. acknowledges support by the EPF Lausanne. Y.M. acknowledges support by the National Natural Science Foundation of China (Grant No. 21303096). We thank Peter Feulner and Florian Blobner for their help in setting up the UHV chamber.

References

1 S. Yamaguchi and K. Tamao, *J. Chem. Soc., Dalton Trans.*, 1998, 3693–3702.
2 J. Liu, J. Lam and B. Tang, *J. Inorg. Organomet. Polym. Mater.*, 2009, **19**, 249–285.
3 J. Luo, Z. Xie, J. W. Y. Lam, L. Cheng, H. Chen, C. Qiu, H. S. Kwok, X. Zhan, Y. Liu, D. Zhu and B. Z. Tang, *Chem. Commun.*, 2001, 1740–1741.
4 Y. Hong, J. W. Y. Lam and B. Z. Tang, *Chem. Soc. Rev.*, 2011, **40**, 5361–5388.
5 E. H. Braye, W. Hübel and I. Caplier, *J. Am. Chem. Soc.*, 1961, **83**, 4406–4413.
6 H. Chen, J. Chen, C. Qiu, B. Tang, M. Wong, H.-S. Kwok, *SID Symposium Digest of Technical Papers*, 2003, 34, 509–511.
7 G. Yu, S. Yin, Y. Liu, J. Chen, X. Xu, X. Sun, D. Ma, X. Zhan, Q. Peng, Z. Shuai, B. Tang, D. Zhu, W. Fang and Y. Luo, *J. Am. Chem. Soc.*, 2005, **127**, 6335–6346.
8 Y. Hong, J. W. Y. Lam and B. Z. Tang, *Chem. Commun.*, 2009, 4332–4353.
9 K. Tamao, M. Uchida, T. Izumizawa, K. Furukawa and S. Yamaguchi, *J. Am. Chem. Soc.*, 1996, **118**, 11974–11975.
10 L. Dong, W. Wang, T. Lin, K. Diller, J. V. Barth, J. Liu, B. Z. Tang, F. Klappenberger and N. Lin, *J. Phys. Chem. C*, 2015, **119**, 3857–3863.
11 A. Thompson, D. Attwood, E. Gullikson, M. Howells, K.-J. Kim, J. Kirz, J. Kortright, I. Lindau, Y. Liu, P. Pianetta, A. Robinson, J. Scofield, J. Underwood and G. Wiliams, *X-ray data booklet, Lawrence Berkeley National Labaratory*, University of California, 3rd edn, 2009.
12 J. Stöhr, *NEXAFS Spectroscopy*, Springer, 1992.
13 C. Lee, W. Yang and R. G. Parr, *Phys. Rev. B: Condens. Matter Mater. Phys.*, 1988, **37**, 785–789.
14 M. J. Frisch, G. W. Trucks, H. B. Schlegel, G. E. Scuseria, M. A. Robb, J. R. Cheeseman, G. Scalmani, V. Barone, B. Mennucci, G. A. Petersson, H. Nakatsuji, M. Caricato, X. Li, H. P. Hratchian, A. F. Izmaylov, J. Bloino, G. Zheng, J. L. Sonnenberg, M. Hada, M. Ehara, K. Toyota, R. Fukuda, J. Hasegawa, M. Ishida, T. Nakajima, Y. Honda, O. Kitao, H. Nakai, T. Vreven, J. A. Montgomery Jr, J. E. Peralta, F. Ogliaro, M. Bearpark, J. J. Heyd, E. Brothers, K. N. Kudin, V. N. Staroverov, R. Kobayashi, J. Normand, K. Raghavachari, A. Rendell, J. C. Burant, S. S. Iyengar, J. Tomasi, M. Cossi, N. Rega, J. M. Millam, M. Klene, J. E. Knox, J. B. Cross, V. Bakken, C. Adamo, J. Jaramillo, R. Gomperts, R. E. Stratmann, O. Yazyev, A. J. Austin, R. Cammi, C. Pomelli, J. W. Ochterski, R. L. Martin, K. Morokuma, V. G. Zakrzewski, G. A. Voth, P. Salvador, J. J. Dannenberg, S. Dapprich, A. D. Daniels, O. Farkas, J. B. Foresman, J. V. Ortiz, J. Cioslowski and D. J. Fox, *Gaussian 09 revision A.02*, Gaussian Inc., Wallingford CT, 2009.
15 K. Hermann, L. Pettersson, M. Casida, C. Daul, A. Goursot, A. Koester, E. Proynov, A. St-Amant, D. S. C. V. Carravetta, H. Duarte, C. Friedrich, N. Godbout, J. Guan, C. Jamorski, M. Leboeuf, M. Leetmaa, M. Nyberg, S. Patchkovskii, L. Pedocchi, F. Sim, L. Triguero and A. Vela, *StoBe-deMon version 3.0*, http://w3.rz-berlin.mpg.de/ hermann/StoBe/ index.html, 2007.
16 L. Triguero, O. Plashkevych, L. G. M. Pettersson and H. Ågren, *J. Electron Spectrosc. Relat. Phenom.*, 1999, **104**, 195–207.
17 P. S. Bagus, *Phys. Rev.*, 1965, **139**, A619.
18 P. W. Langhoff, in *Electron Molecule and Photon Molecule Collisions*, ed. T. N. Rescigno, B. V. McKoy and B. Schneider, Plenum, New York, 1979, p. 183.
19 P. W. Langhoff and C. T. Corcoran, *J. Chem. Phys.*, 1974, **61**, 146.
20 P. W. Langhoff, C. T. Corcoran, J. S. Sims, F. Weinhold and R. M. Glover, *Phys. Rev. A: At., Mol., Opt. Phys.*, 1976, **14**, 402.
21 A. D. Becke, *Phys. Rev. A: At., Mol., Opt. Phys.*, 1988, **38**, 3098–3100.
22 J. P. Perdew, *Phys. Rev. B: Condens. Matter Mater. Phys.*, 1986, **33**, 8822.
23 L. Triguero, L. G. M. Pettersson and H. Ågren, *Phys. Rev. B: Condens. Matter Mater. Phys.*, 1998, **58**, 8097.
24 W. Kutzelnigg, U. Fleischer and M. Schindler, *NMR Basic Principles and Progress*, Springer Verlag, Heidelberg, 1990, vol. 23.
25 R. S. Mulliken, *J. Chem. Phys.*, 1955, **23**, 1833–1840.
26 H. Lu, D. Dai, P. Yanga and L. Lic, *Phys. Chem. Chem. Phys.*, 2006, **8**, 340–346.
27 A. E. Reed, R. B. Weinstock and F. Weinhold, *J. Chem. Phys.*, 1985, **83**, 735.
28 M. Alexander, R. Short, F. Jones, W. Michaeli and C. Blomfield, *Appl. Surf. Sci.*, 1999, **137**, 179–183.
29 J.-K. Choi, S. Jang, K.-J. Kim, H. Sohn and H.-D. Jeong, *J. Am. Chem. Soc.*, 2011, **133**, 7764–7785.
30 S. Lee, S. Makan, M. M. Banaszak Holl and F. R. McFeely, *J. Am. Chem. Soc.*, 1994, **116**, 11819–11826.
31 Y. Hijikata, H. Yaguchi, M. Yoshikawa and S. Yoshida, *Appl. Surf. Sci.*, 2001, **184**, 161–166.
32 J. H. Xu, J. V. Mallow and M. A. Ratner, *J. Phys. B: At., Mol. Opt. Phys.*, 1983, **16**, 3863–3872.
33 S. Gronert, R. Glaser and A. Streitwieser, *J. Am. Chem. Soc.*, 1989, **111**, 3111–3117.
34 F. Klappenberger, D. Kühne, M. Marschall, S. Neppl, W. Krenner, A. Nefedov, T. Strunskus, K. Fink, C. Wöll, S. Klyatskaya, O. Fuhr, M. Ruben and J. V. Barth, *Adv. Funct. Mater.*, 2011, **21**, 1631–1642.
35 R. Nordberg, H. Brecht, R. G. Albridge, A. Fahlman and J. R. Van Wazer, *Inorg. Chem.*, 1970, **9**, 2469–2474.

36 R. Gray, J. Carver and D. Hercules, *J. Electron Spectrosc. Relat. Phenom.*, 1976, **8**, 343–357.
37 G. Iucci, V. Carravetta, P. Altamura, M. V. Russo, G. Paolucci, A. Goldoni and G. Polzonetti, *Chem. Phys.*, 2004, **302**, 43–52.
38 H. Hoffmann, F. Zaera, R. Mark Ormerod, R. M. Lambert, L. P. Wang and W. T. Tysoe, *Surf. Sci.*, 1990, **232**, 259–265.
39 K. Diller, F. Klappenberger, M. Marschall, K. Hermann, A. Nefedov, C. Wöll and J. V. Barth, *J. Chem. Phys.*, 2012, **136**, 014705-13.
40 Y. Ning, J. Jiang, Z. Shi, Q. Fu, J. Liu, Y. Luo, B. Z. Tang and N. Lin, *J. Phys. Chem. C*, 2009, **113**, 26–30.
41 G. Hähner, *Chem. Soc. Rev.*, 2006, **35**, 1244–1255.
42 M. Xi, M. X. Yang, S. K. Jo, B. E. Bent and P. Stevens, *J. Chem. Phys.*, 1994, **101**, 9122–9131.
43 R. Püttner, C. Kolczewski, M. Martins, A. S. Schlachter, G. Snell, M. Sant'Anna, J. Viefhaus, K. Hermann and G. Kaindl, *Chem. Phys. Lett.*, 2004, **393**, 361–366.
44 U. Ekström, H. Ottosson and P. Norman, *J. Phys. Chem. C*, 2007, **111**, 13846–13850.
45 D. Li, G. M. Bancroft, M. Kasrai, M. E. Fleet, R. A. Secco, X. H. Feng, K. H. Tan and B. X. Yang, *Am. Mineral.*, 1994, **79**, 622–632.
46 S. G. Urquhart, C. C. Turci, T. Tyliszczak, M. A. Brook and A. P. Hitchcock, *Organometallics*, 1997, **16**, 2080–2088.
47 J. Z. Xiong, D. T. Jiang, Z. F. Liu, K. M. Baines, T. K. Sham, S. G. Urquhart, A. T. Wen, T. Tyliszczak and A. P. Hitchcock, *Chem. Phys.*, 1996, **203**, 81–92.
48 D. Käfer, L. Ruppel, G. Witte and C. Wöll, *Phys. Rev. Lett.*, 2005, **95**, 166602.

